Proceedings of HT-FED04
2004 ASME Heat Transfer/Fluids Engineering Summer Conference
July 11-15, 2004, Charlotte, North Carolina USA

HT-FED04-56813

AN ASSESSMENT OF FIVE TURBULENCE MODELS IN PREDICTING TURBULENT SEPARATION

Robert E. Spall
Warren F. Phillips
Nick Alley
Department of Mechanical and Aerospace Engineering
UMC 4130
Utah State University
Logan, UT 84322-4130
spall@engineering.usu.edu
wfphillips@engineering.usu.edu

ABSTRACT

Four different turbulence models were employed to predict the flow over a wall-mounted Glauert-Goldschmied body. The models evaluated include: 1) two-layer $k-\varepsilon$, 2) shear stress transport, 3) low-Reynolds number $k-\omega$, 4) Spalart-Allmaras, and 5) v^2-f. Calculations were performed for both an uncontrolled case, and a controlled-flow case which used steady suction through a slot located at the 65% chord station. The flow conditions include a freestream Mach number of approximately 0.1, and a chord Reynolds number of just under 1 million. For each model, the numerical results over predicted the experimentally determined re-attachment length. An examination of streamwise velocity profiles at several stations downstream of the trailing edge revealed considerable variation in the predictions of the five turbulence models.

INTRODUCTION

The NASA Langley Research Center Workshop on CFD Validation of Synthetic Jets and Turbulent Separation Control was held March 29-31, 2004 in Williamsburg, VA. The purpose of the workshop was to assess the current capabilities of different classes of turbulent flow methodologies to predict flow fields induced by synthetic jets and separation control geometries. Three different test cases were examined at the workshop: 1) synthetic jet into a quiescent air, 2) synthetic jet in a crossflow, and 3) flow over a "hump" model. Solution methodologies represented include large-eddy simulations, detached-eddy simulations, and Reynolds-averaged Navier-Stokes (RANS) simulations.

The results presented herein involve RANS solutions to Case 3. The model represents a Glauert-Goldschmied body which is geometrically similar to that employed by Seifert and Pack [1]. The commercial CFD solver Fluent (Fluent, Inc., Lebanon, NH) was used to obtain results for five different turbulence models: 1) two-layer $k-\varepsilon$, 2) shear stress transport (SST), 3) low-Reynolds number $k-\omega$, 4) Spalart-Allmaras, and 5) v^2-f. Experimental data, with which comparisons have been made, are available on the workshop web site: `http://cfdval2004.larc.nasa.gov/case3.html`.

TURBULENCE MODEL DESCRIPTIONS

A brief description of each model appears below, with an emphasis on describing methodology that often varies within each class of model. We note that in all cases, the near wall mesh within the channel region along the lower wall was sufficiently fine so that wall functions were never implemented.

1) The $k-\varepsilon$ model

The $k-\varepsilon$ model of Launder and Spalding [2] was employed, with low-Reynolds number modifications for the near-wall modeling, which combine a two-layer model with wall functions. In the present work, the near wall mesh was fine enough to resolve the viscous sublayer; consequently the two-layer model was used and wall functions were never implemented. In particular, if $Re_y < Re_y^*$ (where $Re_y^* = 200$ and $Re_y = \rho y\sqrt{k}/\mu$) the one-equation model of Wolfstein [3] is employed. In this region, the equation for k is retained, but the turbulent viscosity is obtained from $\mu_{t,i} = \rho C_\mu l_\mu \sqrt{k}$ where the length scale is given as $l_\mu = yc_l(1-e^{-Re_y/A_\mu})$ [4]. The turbu-

lent viscosity determined above is then smoothly blended with the high Reynolds number turbulent viscosity, $\mu_{t,o}$, obtained in the outer region. The dissipation rate in the near wall region is also specified algebraically as $\varepsilon = k^{3/2}/l_\varepsilon$ where the length scale, l_ε, is computed using the same relation used in the specification of the turbulent viscosity, although with a different value of the constant, A. A blending function is used to ensure a smooth transition between ε specified algebraically in the inner region, and ε computed via the transport equation in the outer region. The blending is of the form:

$$\mu_t = \lambda\mu_{t,o} + (1-\lambda)\mu_{t,i} \quad [1]$$

where,

$$\lambda = \frac{1}{2}\left[1 + \tanh\frac{(Re_y - Re_y^*)}{A}\right] \quad [2]$$

2) The $k-\omega$ model

A low-Reynolds number version of the Wilcox $k-\omega$ model [5] was employed. In particular, a low-Reynolds number correction to the turbulent viscosity, $\mu_t = \alpha^*\rho k/\omega$, is determined as:

$$\alpha^* = \alpha_\infty^*\left(\frac{\alpha_0^* + Re_t/R_k}{1 + Re_t/R_k}\right) \quad [3]$$

where $Re_t = (\rho k)/(\mu\omega)$, $R_k = 6$, $\alpha_0^* = \beta_i/3$, $\alpha_\infty^* = 1$, and $\beta_i = 0.072$. A low-Reynolds number correction is also applied to the ω production term, $G_\omega = \alpha\omega G_k/k$, (where G_k is the production term of turbulence kinetic energy) as:

$$\alpha = \frac{\alpha_\infty}{\alpha^*}\left(\frac{\alpha_0 + Re_t/R_\omega}{1 + Re_t/R_\omega}\right) \quad [4]$$

where $\alpha_\infty = 0.52$ and $R_\omega = 2.95$. The asymptotic value of ω at the wall is specified as:

$$\omega_w = \rho(u^*)^2\omega^+/\mu \quad [5]$$

The value of ω^+ is determined from:

$$\omega^+ = \min\left[2500, \frac{6}{\beta_\infty^*(y^+)^2}\right] \quad [6]$$

where $\beta_\infty^* = 0.09$.

3) Spalart-Allmaras model

The Spalart-Allmaras model [6] solves a transport equation for a variable that is a modified form of the turbulent kinematic viscosity. For the results presented, the deformation tensor, *S*, appearing in the production term follows the original model proposed by Spalart and Allmaras, which is based on the magnitude of the vorticity $S = \sqrt{2\Omega_{ij}\Omega_{ij}}$, where Ω_{ij} is the mean rate-of-rotation tensor. Fluent also incorporates a modified definition of *S* which includes measures of both rotation and strain tensors in its definition; however, this modification was not used.

4) Shear stress transport model

The results presented employed a low-Reynolds number version of the shear stress transport model [7]. In particular, the turbulent viscosity was determined as:

$$\mu_t = \frac{\rho k}{\omega}\frac{1}{\max\left[\frac{1}{\alpha^*}, \frac{\Omega F_2}{\alpha_1\omega}\right]} \quad [7]$$

where α^* is as defined for the $k-\omega$ model and $\Omega = \sqrt{2\Omega_{ij}\Omega_{ij}}$. In addition, the turbulent Prandtl numbers are defined as:

$$\sigma_k = \frac{1}{F_1/\sigma_{k,1} + (1-F_1)/\sigma_{k,2}} \quad [8]$$

$$\sigma_\omega = \frac{1}{F_1/\sigma_{\omega,1} + (1-F_1)/\sigma_{\omega,2}} \quad [9]$$

where F_1 and F_2 are blending functions. In addition, $\sigma_{k,1}$ and $\sigma_{k,2}$ are constant inner and outer turbulent Prandtl numbers, respectively. (Similarly for $\sigma_{\omega,1}$ and $\sigma_{\omega,2}$.)

5) The $v^2 - f$ model

The $v^2 - f$ model, which is not as commonly used as other turbulence models, was developed from a simplified second-moment closure approach, and involves the solution of three transport equations for the turbulence quantities k, ε, and v^2, and an elliptic equation for near wall and non-local effects [8]. The model extends the standard $k-\varepsilon$ model by incorporating near-wall turbulence anisotropy while retaining a linear eddy viscosity approximation. The v^2 term is taken as the velocity scale for the evaluation of the turbulent viscosity; it is proportional to k far from the wall, but in the near-wall region it represents the velocity fluctuation normal to the surface. Alternative formulations of the $v^2 - f$ model, which address deficiencies identified in the earlier models, have recently been developed. For instance, the Cokljat et al. [9] formulation, which is implemented in Fluent, utilizes homogeneous boundary conditions on the elliptic function, f, to improve robustness.

SOLUTION METHODOLOGY

As stated previously, the results were computed using the commercial CFD solver Fluent (version 6.18). Fluent employs a pressure-based finite volume solution procedure to solve the governing equations on unstructured grids. Pressure-velocity coupling was accomplished using the SIMPLEC procedure.

Second-order central differencing was used for the viscous terms in the transport equations. Interpolation to cell faces for the convection terms was performed using a third-order QUICK scheme. In all cases, a steady, two-dimensional formulation was employed. Solutions obtained using a segregated solver were considered converged when residuals for each of the equations (based on an L2 norm) were reduced by a minimum of five orders of magnitude. Additional iterations were then performed to confirm iterative convergence.

GEOMETRY and BOUNDARY CONDITIONS

The width of the experimental model was sufficiently large that the experimental results are nominally two-dimensional. An outline of the corresponding computational domain is shown in Fig. 1. Further details of the model geometry are available on the aforementioned web site.

Relevant free-stream flow conditions are given as $M_\infty = 0.1$ and $Re_\infty = 2.23x10^6/m$. For the flow-control case, the chamber suction rate was specified as $0.02598 kg/s$ (per meter width). For the no-flow-control case, zero mass flow was specified at the inlet to the suction chamber. However, the passage to the main channel was left open. The inlet *u*-velocity boundary condition was specified using the experimental profile available on the workshop web site. The *v*-velocity was set to zero. Turbulence quantities were derived from the approximate inlet turbulence intensity (I) of 0.09% (given on web site) and a turbulence length scale (l) which was defined as $0.4\delta_{0.99}$ (where $\delta_{0.99}$ is the boundary layer thickness at the inlet). In particular, the inlet turbulence kinetic energy was set to $k = 1.5(\bar{u}I)^2$ where $\bar{u}$ is the mean flow velocity. The dissipation rate was computed as $\varepsilon = C_\mu^{3/4} k^{3/2}/l$. For the Spalart-Allmaras model, the inlet modified viscosity was specified using a length scale and turbulence intensity as $\tilde{\nu} = \sqrt{3/2}\bar{u}Il$. When implementing the $k-\omega$ model, the inlet specific dissipation rate was computed from $\omega = k^{1/2}/(C_\mu^{1/4} l)$. In all cases, zero normal derivative boundary conditions were used at the outflow plane. No-slip conditions were implemented on both the upper and lower walls. The model-specific approaches to implementing wall boundary conditions were described in the section, Turbulence Model Descriptions. (We note that slip-wall conditions were also used on the upper wall, with little change in the resulting solutions. However, the results presented are for the no-slip conditions.)

Solutions were computed on two different grids. The coarser grid consisted of 38,720 quadrilateral cells; the finer grid consisted of 85,760 cells. Grid points were clustered toward the wall so that in all cases $y^+ < 0.5$ for the lower wall adjacent cells. This was achieved by specifying the distance of the first grid point above the lower wall as $y = 0.000018c$ (where c is the chord length). The grid spacing along the upper wall was defined such that $y^+ \approx 50$, so that wall functions were used. For both flow-control and no-flow-control cases, the suction chamber was included in the model and contained 2,169 tetrahedral cells. No grid refinement was performed within the suction chamber. The grids (either fine or coarse) within the channel and chamber were identical for both the no-flow-control and flow-control cases.

RESULTS

We show in Figs. 2 and 3 contours of streamlines in the area of the separation downstream of the hump, computed using the two-layer $k-\varepsilon$ model. The results provide a global view of the flow patterns in the separated region, and the extent to which the flow control decreases the extent of the separation zone. In particular, the initial point of separation for the flow-control case moves downstream only a small distance relative to the no-flow-control results. However, the length of the recirculation zone is considerably reduced. These results are consistent with experimental observations.

This behavior is further quantified by examining reattachment points for each model as shown in Table 1. The experimentally determined reattachment points, determined using an oil film technique, are given as $x/c = 1.11 \pm 0.003$ and $x/c = 0.94 \pm 0.005$ for the no-flow-control and flow-control cases, respectively. Consequently, all models over predicted the length of the separation region for both the no-flow-control and flow-control cases. In particular, the results indicate that the $k-\varepsilon$ model performed best, predicting the no-flow-control case to within 3% (chord length) of the experimentally determined value and the flow-control case to within 7% of the experimental value. The worst performing model, the v^2-f model, was in error by approximately 19% for the no-flow-control case, and approximately 30% for the flow-control case.

Shown in Figs. 4 and 5 are line plots of pressure coefficient vs. x/c for no-flow-control and flow-control cases, respectively. Experimental data downloaded from the workshop web site are also included on the figures. For the no-flow-control case, each model over predicts the experimentally measured pressure rise over the aft section of the hump geometry (i.e., downstream of the suction slot bounded by $0.654 \le x/c \le 0.658$). Most models performed in a similar manner; the exceptions being the $k-\varepsilon$ model which predicted a larger pressure recovery, and the v^2-f model which predicted a smaller pressure recovery. Similar results were found for the flow-control case, with the $k-\varepsilon$ model predicting a larger pressure rise than was predicted by the other models. In general, predictions were in much better agreement with experimental data in the regions upstream of the suction slot.

Shown in Figs. 6 and 7 are friction coefficients along the lower wall for each of the five turbulence models. In each case, the $k-\omega$ model predicted higher levels of the skin friction coefficient than was predicted by the other four models. Considerable variation in c_f is also observed in the region of the hump just upstream of the suction slot.

We show in Figs. $8-11$ mean streamwise velocity profiles at x/c = 1.0 and 1.3, for both no-flow-control and flow-control cases. Experimental data points downloaded from the workshop web site are also included on each of the figures. The results at x/c = 1.0 for the no-flow-control case (shown in Fig. 8) reveal that the $k-\varepsilon$ and $k-\omega$ models do the best job of predicting the experimental profile over the majority of boundary-layer thickness. In the near-wall region, the $k-\varepsilon$ model slightly under predicts the magnitude of the streamwise velocity, while the other models slightly over predict its magnitude. The results for the case with flow control at x/c = 1.0 are shown in Fig. 9, and reveal a degradation in the predictive capability of each model, relative to the no-flow-control case. In particular, the models predict reversed flow where, in fact, the experimental data reveals that this location is downstream of the reattachment location. Similar results are shown in Figs. 8 and 9 for no-flow-control and flow-control cases, respectively, at x/c = 1.3. For the no-flow-control case, the $k-\varepsilon$ and $k-\omega$ models clearly perform the best. For all models, the numerical solutions predict reasonably well the thickness of the boundary layer. For the flow-control case, the $k-\varepsilon$ and $k-\omega$ models somewhat under predict the velocity in the near-wall region. However, the Spalart-Allmaras and shear stress transport models considerably under predict the near-wall velocity.

We present in Figs. $12-15$ both numerical and (workshop) experimental results for the normalized Reynolds shear stress, $\overline{u'v'}/\bar{u}^2$, at locations x/c = 1.0 and 1.3. The Spalart-Allmaras model performs somewhat better than the other models, particularly at locations within the boundary-layer below the location of maximum shear stress. For all cases, the $k-\omega$ model significantly over predicts the maximum levels of shear stress. In addition, the stress levels for the $k-\omega$ model do not recover to zero near the edge of the boundary layer. This difficulty is likely related to the well-known sensitivity of the $k-\omega$ model to free-stream turbulence levels.

CONCLUSIONS

Four different turbulence models were employed to predict the flow over a wall-mounted Glauert-Goldschmied body. The specific geometry was a model of the wall-mounted hump which was included as one of the test cases for the NASA Langley Research Center Workshop on CFD Validation of Synthetic Jets and Turbulent Separation Control. The calculations were performed for both an uncontrolled case, and a controlled-flow case which used steady suction through a slot. For each model, the numerical results over predicted the experimentally determined reattachment length. For the no-flow-control case, differences between experimental and numerical results in the predicted re-attachment point ranged from a low of approximately 3% of the chord length for the standard $k-\varepsilon$ model to a high of 19% for the v^2-f model. However, the $k-\varepsilon$ model was one of the least effective models in predicting the surface pressure coefficient. Overall, we conclude that the $k-\varepsilon$ and $k-\omega$ models performed better than either the Spalart-Allmaras, shear stress transport, or v^2-f models. However, considerable room for improvement in the predictive capability of turbulence models for this separated flow certainly exists.

REFERENCES

[1] Seifert, A. and Pack, L.G., "Active Flow Separation Control on Wall-Mounted Hump at High Reynolds Numbers," *AIAA Journal*, Vol. 40, 2002.

[2] Launder, B.E. and Spalding, D.B., Lectures in Mathematical Models of Turbulence. Academic Press, London, England, 1972.

[3] Wolfstein, M., "The Velocity and Temperature Distribution of One-Dimensional Flow with Turbulence Augmentation and Pressure Gradient," Int. J. Heat Mass Transfer, Vol. 12, pp. 301-318, 1969.

[4] Chen, H.C. and Patel, V.C., "Near-Wall Turbulence Models for Complex Flows Including Separation," *AIAA Journal*, Vol. 26, pp. 641-648, 1988.

[5] Wilcox, D.C., Turbulence Modeling for CFD, DCW Industries, Inc., La Canada, California, 1998.

[6] Spalart, P. and Allmaras, S., "A One-Equation Turbulence Model for Aerodynamic Flows," AIAA-92-0439, 1992.

[7] Menter, F.R., "Improved Two-Equation $k-\omega$ Turbulence Models for Aerodynamic Flows," NASA TM 103975, Oct. 1992.

[8] Durbin, P.A., "Near-Wall Turbulence Closure Modeling Without Damping Functions," *Theoret. Comput. Fluid Dynamics*, Vol. 3, pp. 1-13, 1991.

[9] Cokljat, D., Kim, S.E., Iaccarino, G., and Durbin, P.A., "A Comparative Assessment of the V2F Model for Recirculating Flows," AIAA-2003-0765, 41st Aerospace Sciences Meeting and Exhibit, January 6-9, 2003, Reno, NV.

Table 1: Reattachment points in terms of x/c.

Model	No Flow Control	Flow Control
$k-\varepsilon$	1.144	1.008
$k-\omega$	1.180	1.023
Spalart-Allmaras	1.262	1.130
Shear Stress Transport	1.309	1.117
v^2-f	1.319	1.219
Experiment	1.11	0.94

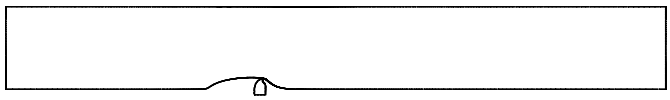

Figure 1. Outline of computational geometry with suction chamber.

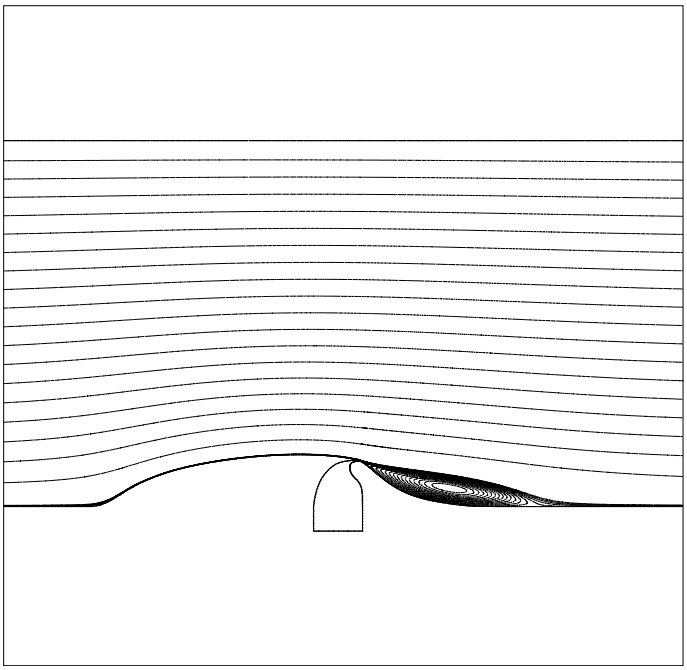

Figure 2. Streamlines in the area of the hump. No flow control.

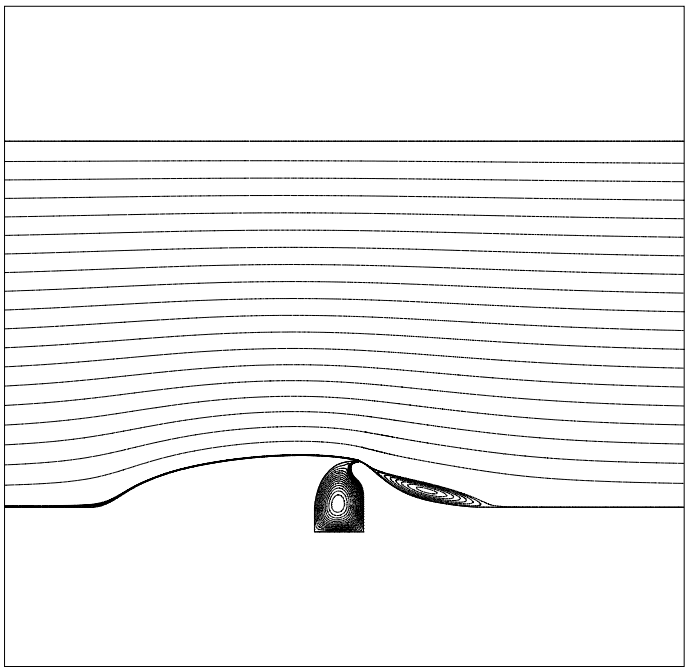

Figure 3. Streamlines in the area of the hump, with flow control.

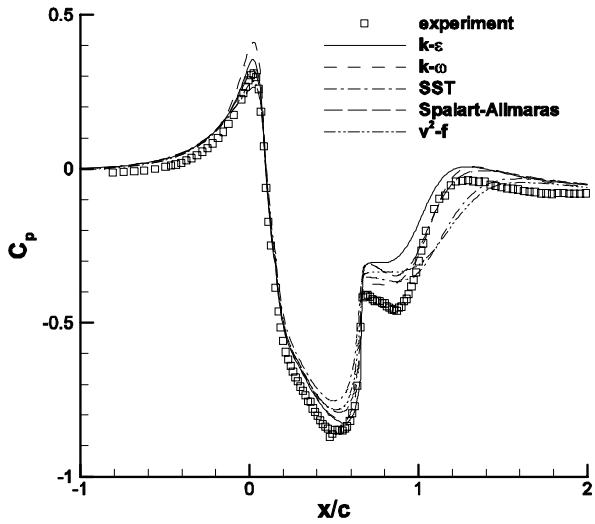

Figure 4. Pressure coefficients without flow control.

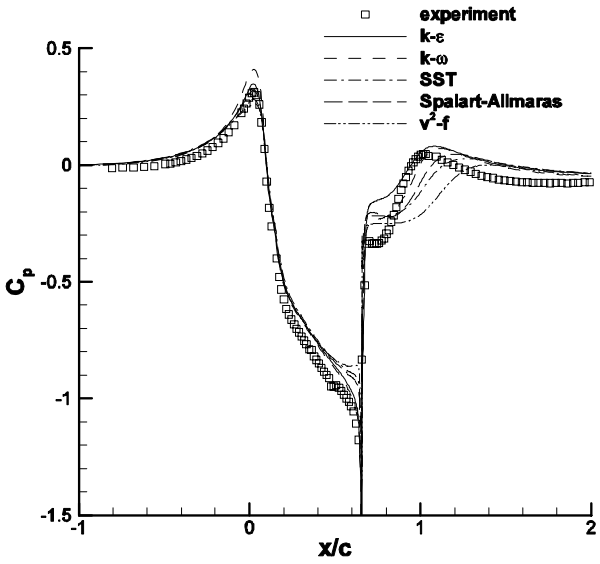

Figure 5. Pressure coefficients with flow control.

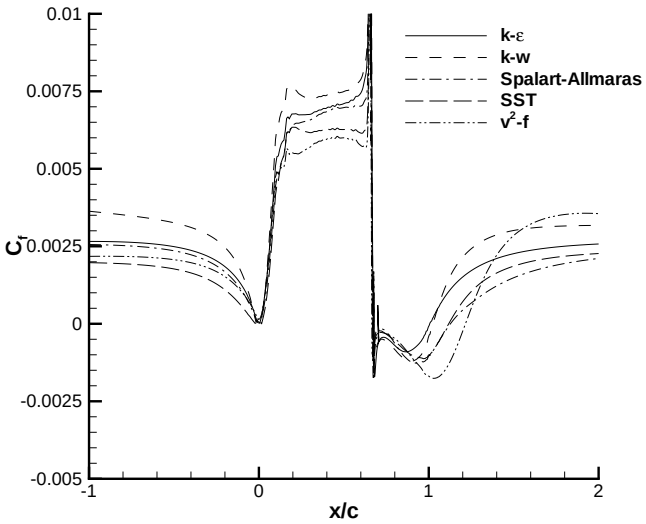

Figure 7. Friction coefficient with flow control.

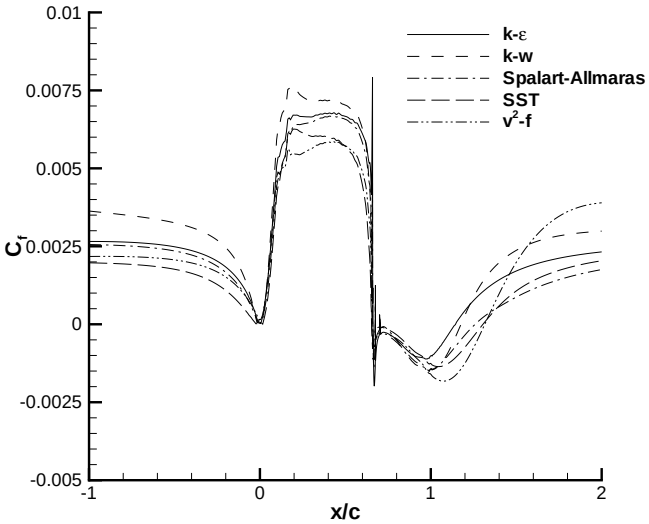

Figure 6. Friction coefficient without flow control.

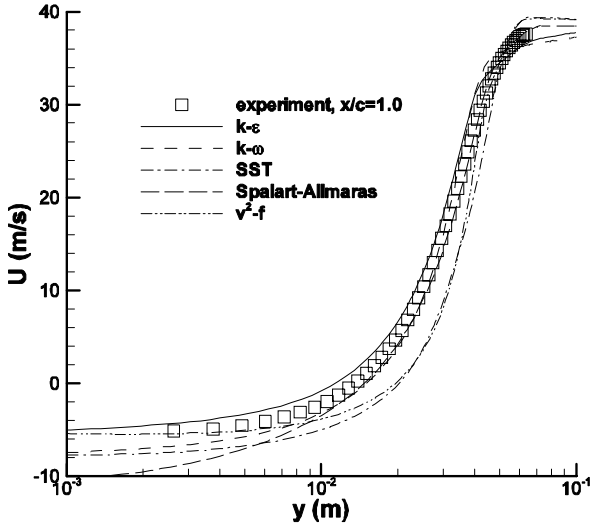

Figure 8. Contours of mean streamwise velocity at $x/c = 1.0$ without flow control.

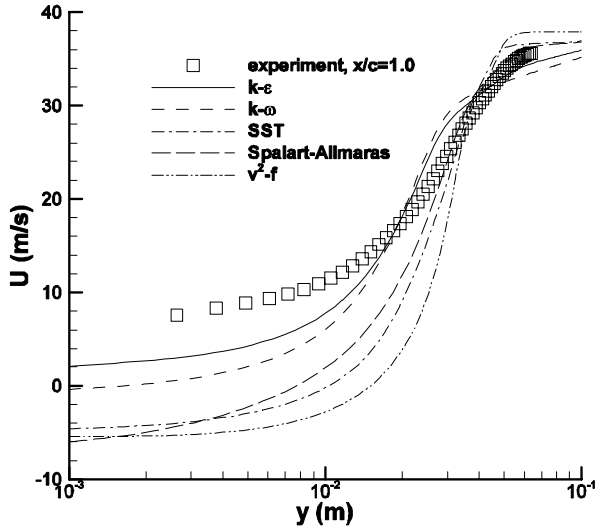

Figure 9. Contours of mean streamwise velocity at x/c = 1.0 with flow control.

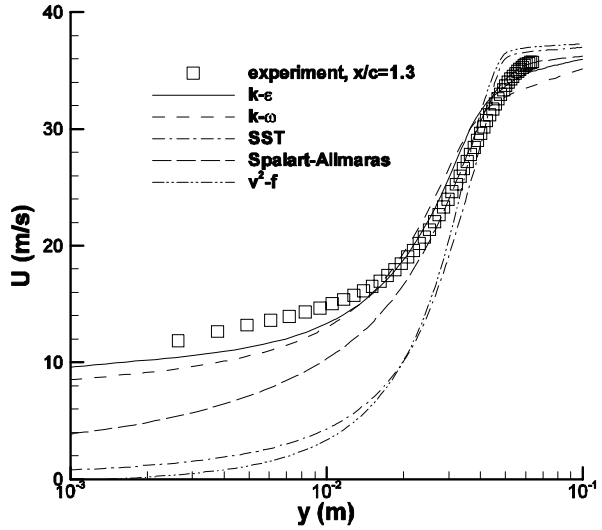

Figure 10. Contours of mean streamwise velocity at x/c = 1.3 without flow control.

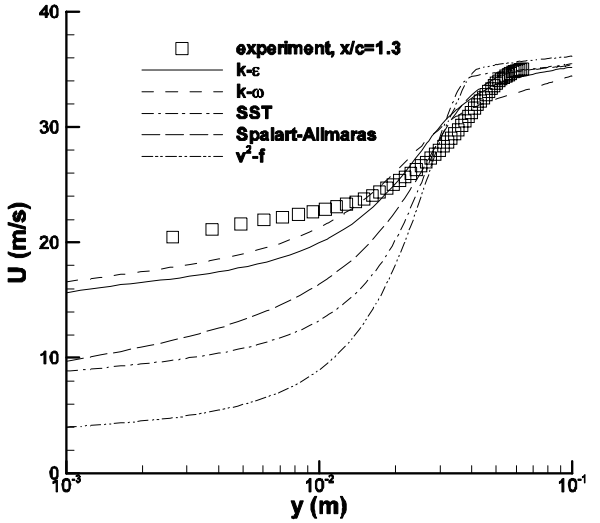

Figure 11. Contours of mean streamwise velocity at x/c = 1.3 with flow control.

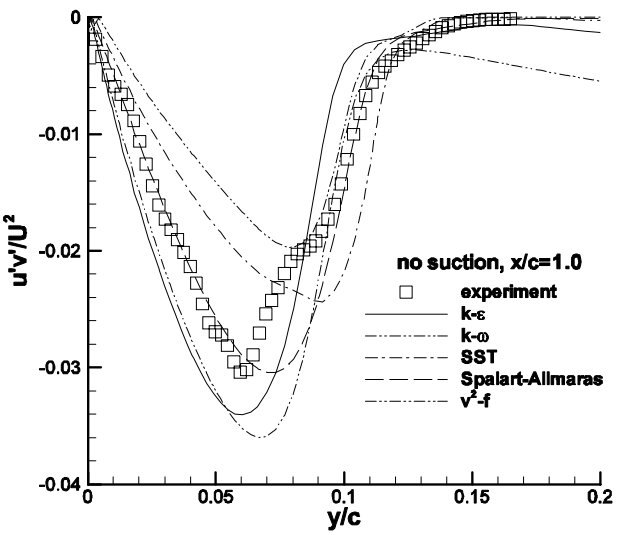

Figure 12. Reynolds shear stress at x/c = 1.0 without flow control.

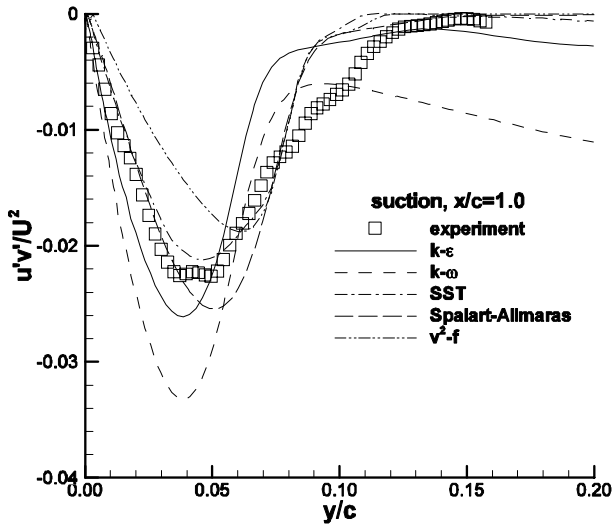

Figure 13. Reynolds shear stress at $x/c = 1.0$ with flow control.

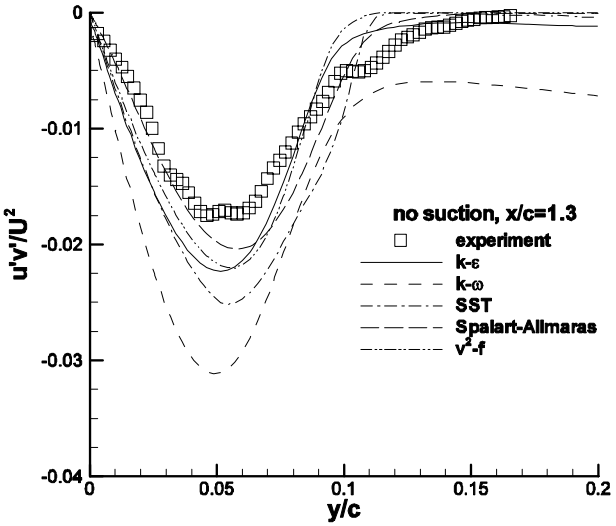

Figure 14. Reynolds shear stress at $x/c = 1.3$ without flow control.

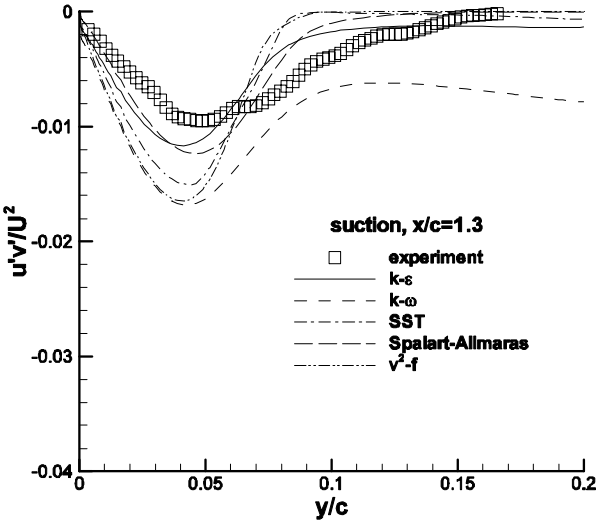

Figure 15. Reynolds shear stress at $x/c = 1.3$ with flow control.